Supporting Information

Highly Ordered 3D Microstructure-Based Electronic Skin Capable of Differentiating Pressure, Temperature, and Proximity

Jin-Oh Kim,[†,#] Se Young Kwon,[†,#] Youngsoo Kim,[‡] Han Byul Choi,[†] Jun Chang Yang,[†] Jinwon Oh,[†] Hyeon Seok Lee,[†] Joo Yong Sim,[§] Seunghwa Ryu,[‡] and Steve Park*,[†]

[†]Department of Materials Science and Engineering, Korea Advanced Institute of Science and Technology (KAIST), Daejeon 34141, Republic of Korea

[‡]Department of Mechanical Engineering, Korea Advanced Institute of Science and Technology (KAIST), Deajeon 34141, Republic of Korea

[§]Bio-Medical IT Convergence Research Department, Electronics and Telecommunications Research Institute (ETRI), Daejeon 34129, Republic of Korea

[#] Equal contribution

[*] Corresponding Author E-mail: stevepark@kaist.ac.kr

Table of Contents

Pressure (kPa)	10	20	30	40	50	60	70	80	90	100
Average of ΔC/Co	4.36551	6.27997	7.48006	8.51076	9.34842	10.03049	10.58601	11.03847	11.41225	11.71143
Standard deviation of ΔC/Co	0.01324	0.00834	0.11579	0.12065	0.12451	0.12765	0.13021	0.13229	0.13401	0.13538
Coefficient of variation (%)	0.3033	0.1328	1.5480	1.4176	1.3319	1.2726	1.2300	1.1984	1.1743	1.1560

Table S1. Average, standard deviation, and coefficient of variation of the relative change in capacitance ($\Delta C/C_0$) under different static pressure levels (10, 20, 30, 40, 50, 60, 70, 80, 90, 100 kPa).

Pressure (kPa)	10	20	30	40	50	60	70	80	90	100
Average of ΔG/Go	3.24045	6.20481	7.74903	9.94411	11.42466	12.63433	13.6423	14.27775	15.04334	15.81872
Standard deviation of ΔG/Go	0.14941	0.23088	0.30625	0.36951	0.02125	0.2866	0.24636	0.01622	0.20727	0.2911
Coefficient of variation (%)	4.611	3.7210	3.9521	3.7159	0.1860	2.2684	1.8059	0.1136	1.3778	1.8402

Table S2. Average, standard deviation, and coefficient of variation of the relative change in conductance ($\Delta G/G_0$) under different static pressure levels (10, 20, 30, 40, 50, 60, 70, 80, 90, 100 kPa).

Temperature (°C)	30	40	50	60	70
Average of ΔR/Ro	-0.04639	-0.10099	-0.16281	-0.25529	-0.3277
Standard deviation of ΔR/Ro	0.00199	0.01174	0.01196	0.01006	0.01739
Coefficient of variation (%)	4.2897	11.6250	7.3460	3.9406	5.3067

Table S3. Average, standard deviation, and coefficient of variation of the relative resistance change ($\Delta R/R_0$) under various temperatures (30, 40, 50, 60, 70 ℃).

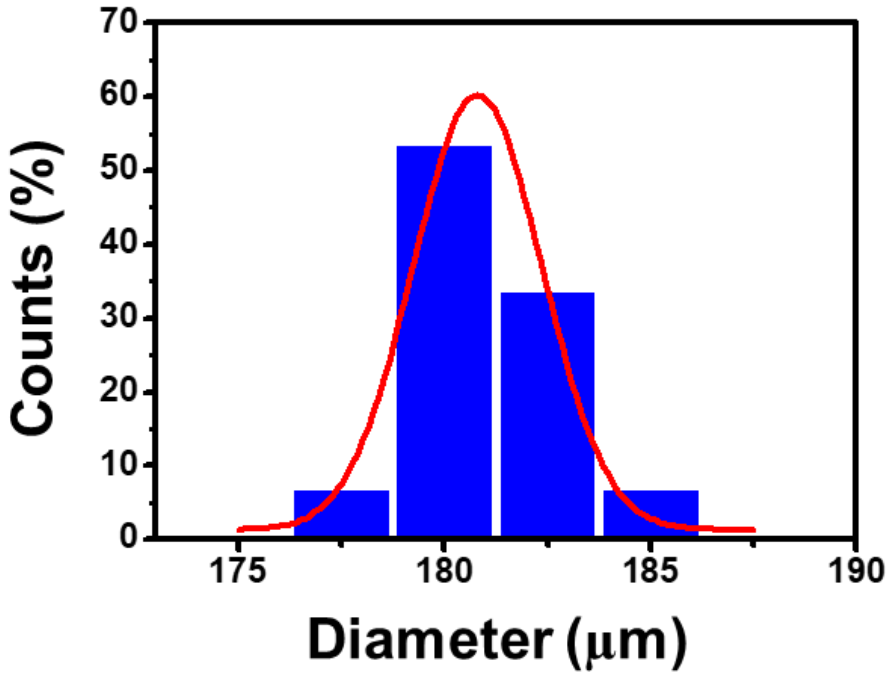

Figure S1. Pore size distribution from SEM image analysis. Mean diameter and standard deviation of the pores were 179.4831 μm and 1.7611 μm, respectively.

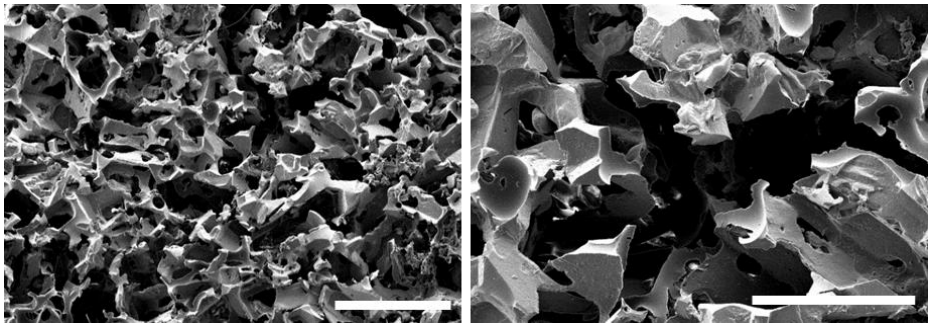

Figure S2. SEM image of sugar template-based microstructure. Scale bar, 1 mm (left) and 500 μm (right).

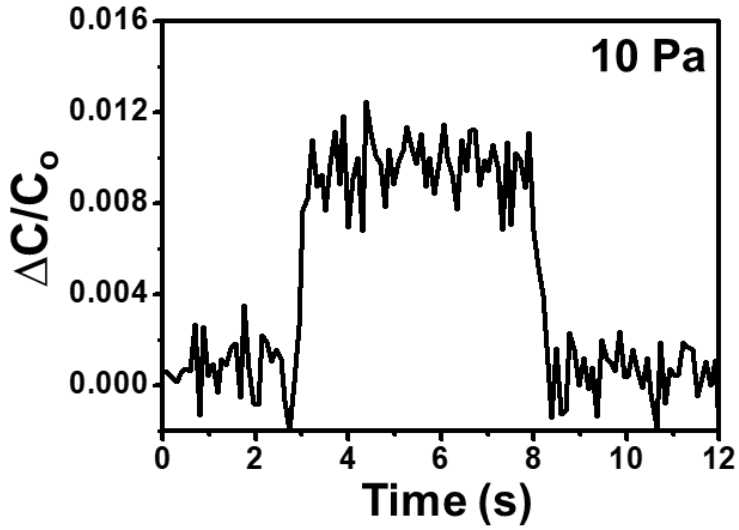

Figure S3. Relative change in capacitance versus time graph with an applied pressure of 10 Pa.

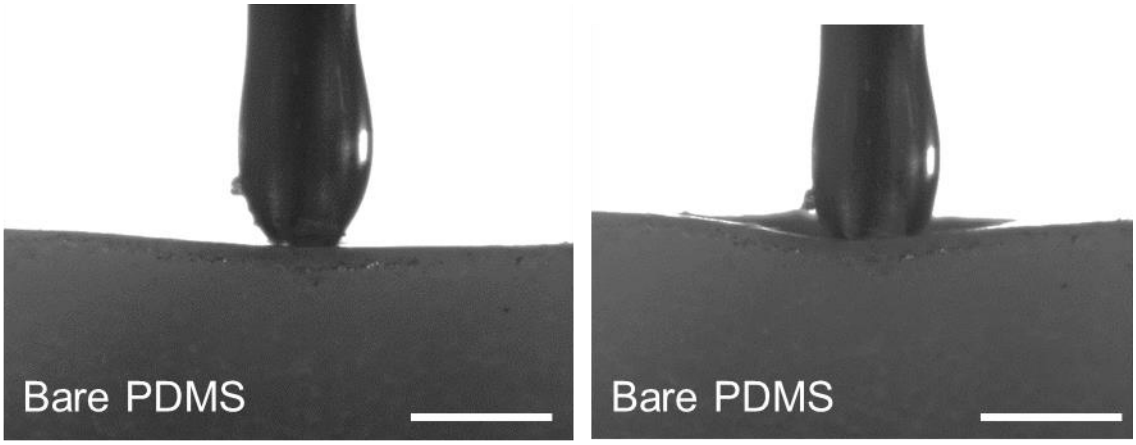

Figure S4. Photographs of a bare PDMS sample pressed by a 1 mm diameter tip under different compressive strains: 0 % (left), 50 % (right). Scale bar, 1 mm.

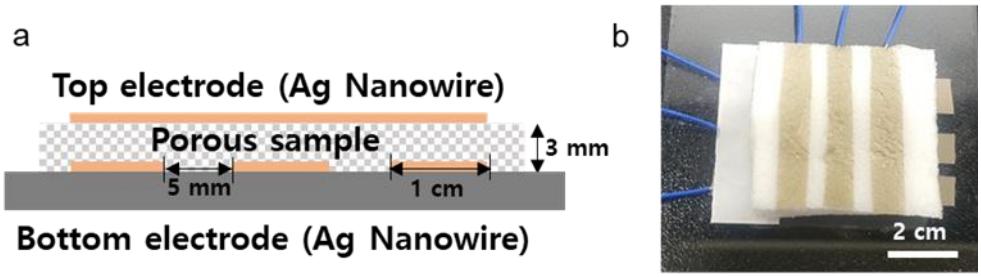

Figure S5. a) Schematic and b) optical image of 3 x 3 array device.

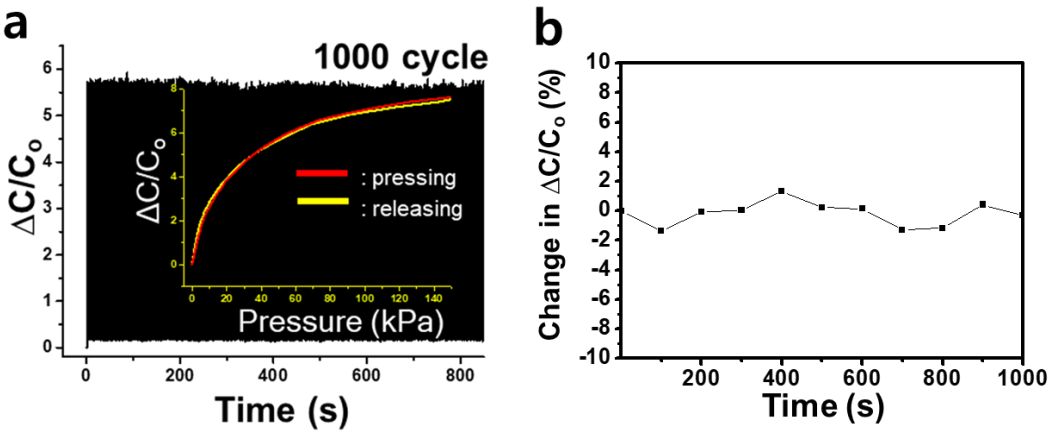

Figure S6. a) Relative capacitance change curve of a 500 μm pore sample under repeated loading and unloading of 70 kPa of pressure for 1000 cycles. The inset is the plot of relative change in capacitance versus pressure under loading and unloading. b) Percentage change in relative capacitance (change in output signal divided by original output signal before cycling) with 1000 cycles.

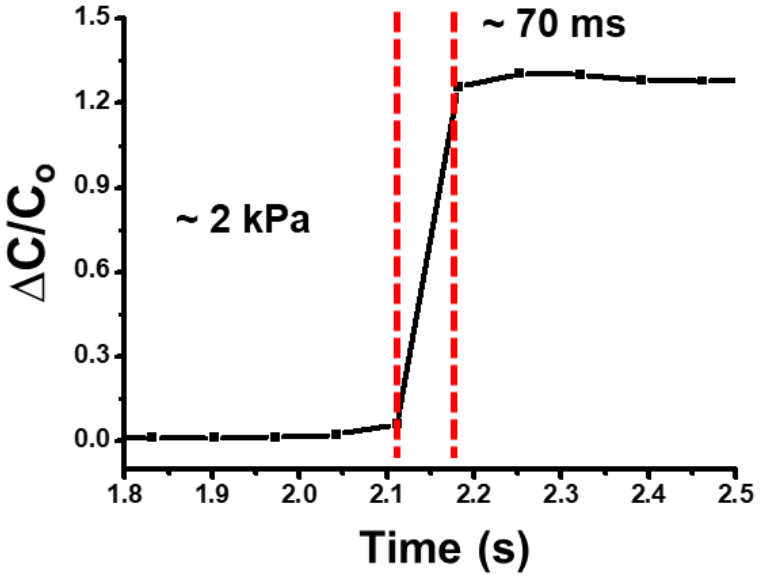

Figure S7. Response time of a 500 μm microporous capacitive sensor upon the loading of 2 kPa of pressure.

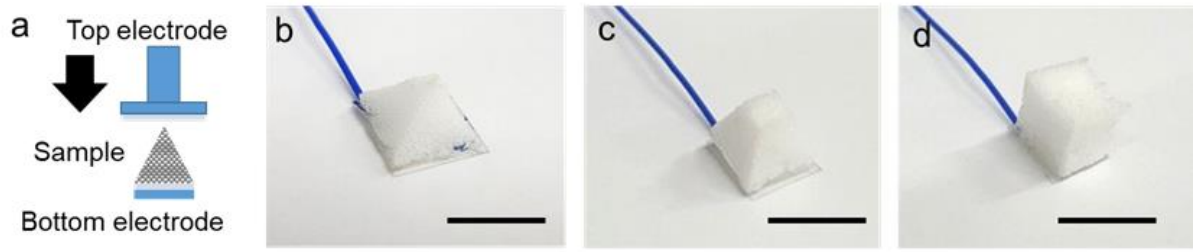

Figure S8. a) Schematic and optical images of different shapes of 3D microstructured elastomers: b) pyramid, c) square horn, d) cuboid. Scale bar, 5 mm.

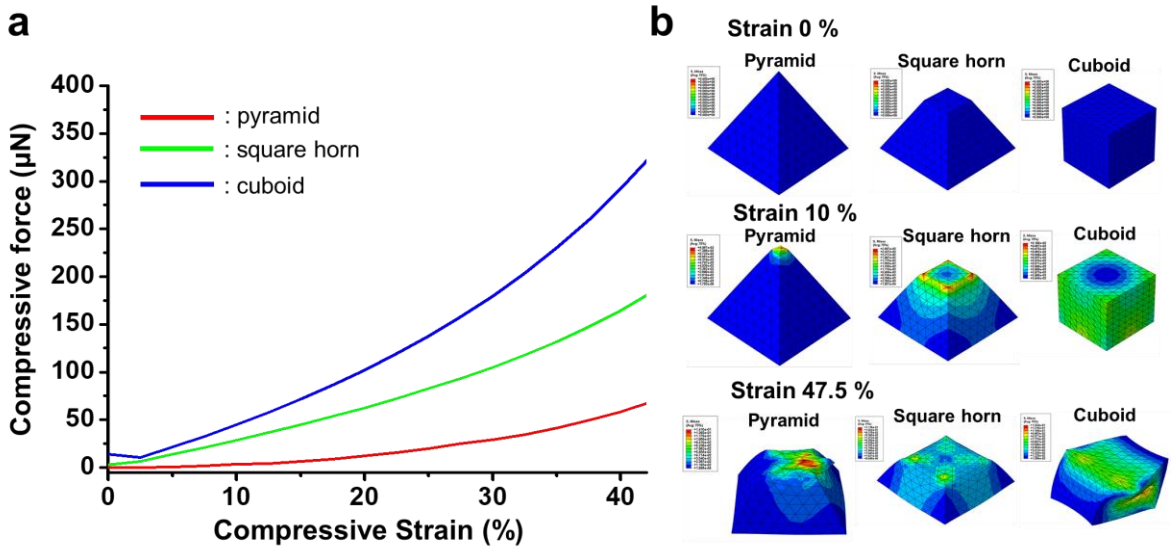

Figure S9. Simulated data of structural effect on the mechanical properties and stress distribution. a) Simulation of compressive force versus compressive strain curves for the differently shaped microstructured samples. b) Simulated images of stress distribution on each sample, under different compressive strains: 0 %, 10 %, and 47.5 %.

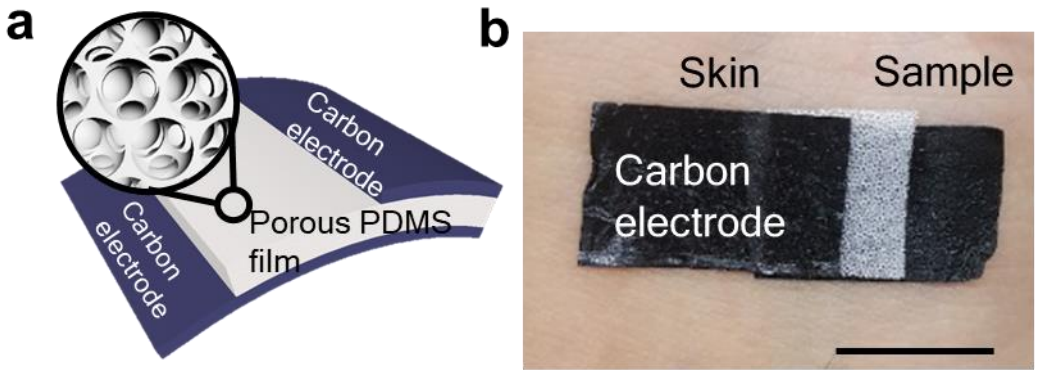

Figure S10. a) Schematic and b) optical image of 3D porous PDMS thin film combined with adhesive carbon electrode. Scale bar, 1 cm.

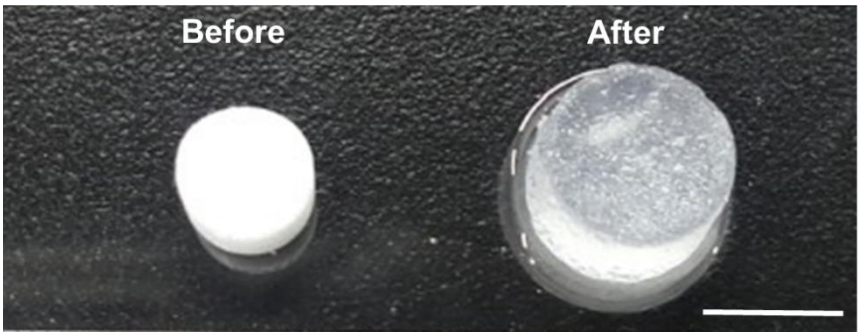

Figure S11. Optical image of microstructured PDMS: before (left) after (right) being swollen by toluene. Scale bar, 1 cm.

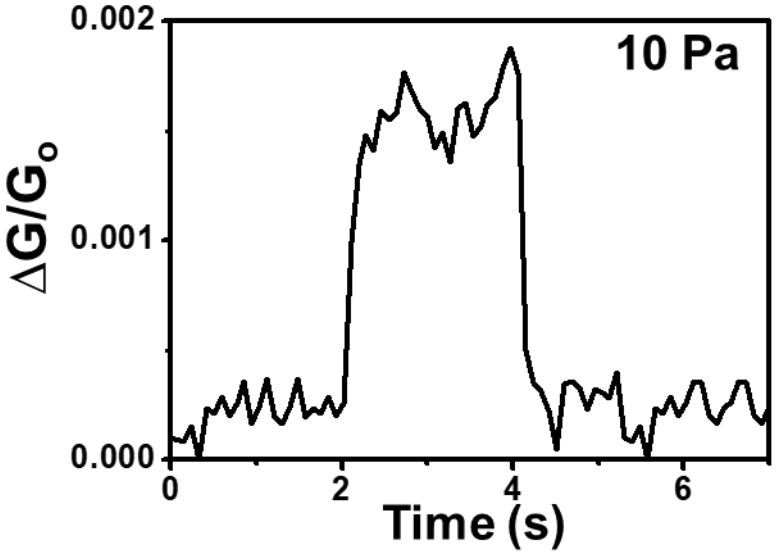

Figure S12. Relative change in conductance versus time graph with an applied pressure of 10 Pa.

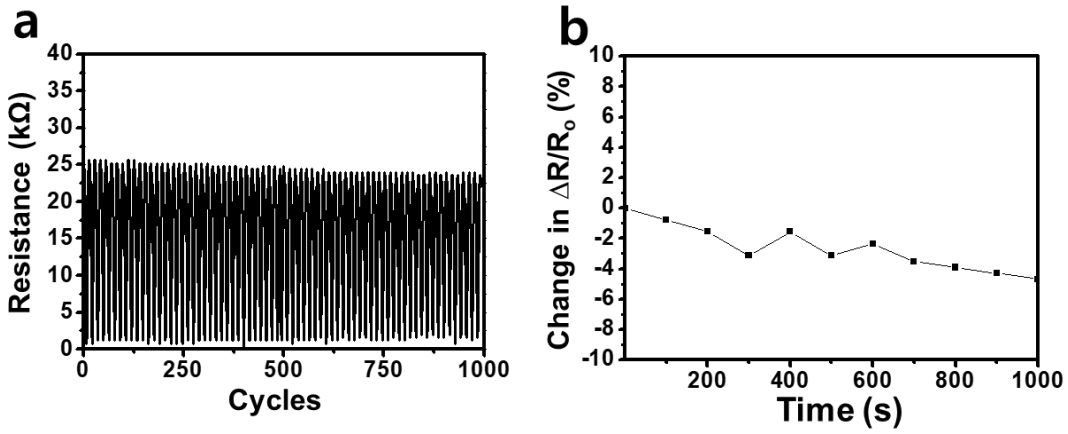

Figure S13. a) Resistance change curve of a 500 μm pore sample under repeated loading and unloading of 70 kPa of pressure for 1000 cycles. b) Percentage change in relative resistance (change in output signal divided by original output signal before cycling) with 1000 cycles.

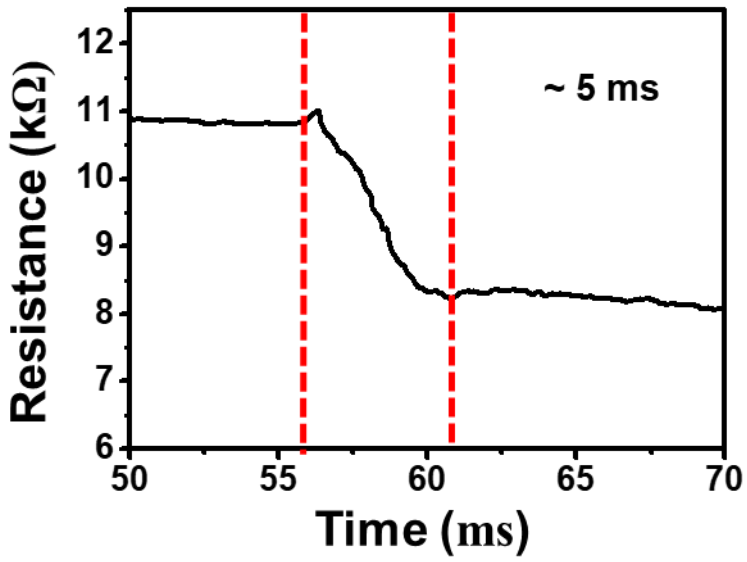

Figure S14. Response time of a 500 μm microporous piezoresistive sensor upon the rapid loading of pressure.

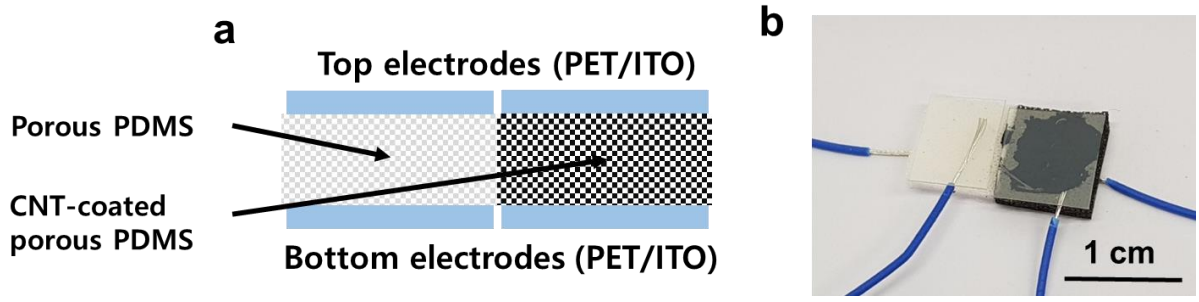

Figure S15. a) Schematic and b) optical image of combined sensor distinguishing temperature, pressure and proximity. Scale bar, 1 cm.

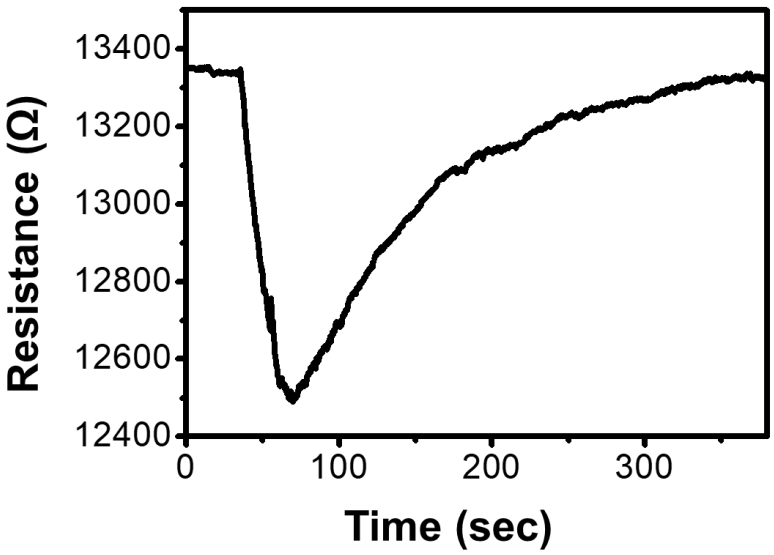

Figure S16. Resistance versus time plot under sudden change in temperature.

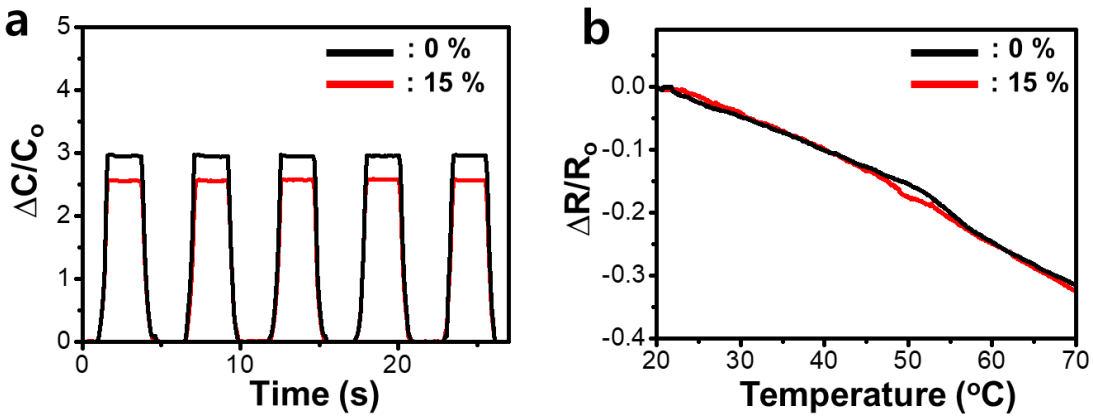

Figure S17. Response of sensor under strain. a) Relative capacitance change versus time plots of our capactive sensor under a repeated pressure of 15 kPa under 0 and 15 % strain. b) Relative resistance change due to temperature of our piezoresistive sensor under 0 and 15 % of strain.